Stopping of Heavy Ion Beams in Dense Plasma of ICF and WDM Concern

C. Deutsch[1] and N.A. Tahir[2]

[1]LPGP UParis-Sud Orsay, France.
[2]GSI 1 Planck Str. Darmstadt, Germany

HIF – 19

UCAL-Berkeley 12-17 Aug. 2012

CONTRIBUTORS :

- M. Barriga-Carrasco, ETS II, UCastilla-la-Mancha, 13071-Ciudad-Real, Spain
- V. Ceban, LPGP, UParis-Sud, Orsay, France
- P. Fromy, CRI, UParis-Sud, Orsay, France
- D. Gilles, CEA/IRFU/SAP, Saclay, France
- D. Léger, Labo Monthouy, UValenciennes-Hainaut Cambresis, France
- G. Maynard, LPGP, UParis-Sud, Orsay, France
- B. Tashev, Dpt Phys, KazNu, Tole BI82, Almaty, Kazakhstan
- L. Volpe, UMilano-Bicocca, 20126 Milano, Italia

- Standard Stopping Model
  (SSM)

- Stopping Plasma Quantitatively Renforced
  (SPQR)

Ion Stopping in Hot-Dense Plasmas

SSM

SPQR

Experimental

PROGRAM

Stopping standard model: basic facts and assumptions

- Intense ion beams appear *dilute* in target
- Rectilinear trajectories
- Pointlike projectiles
- Nonrelativistic regime (ß < 0.35), ß = V_p/C
- $n_e\ell$-scaling $-\Delta E/E = n\ell/E^2$
- Prefactor $4\pi Z_1^2 e^4 n / m_e V_P^2$ dominant for E/A between 1 MeV/amu and 1 GeV/amu
- Log terms dominant at very small (end-of-range) and very large projectile velocity

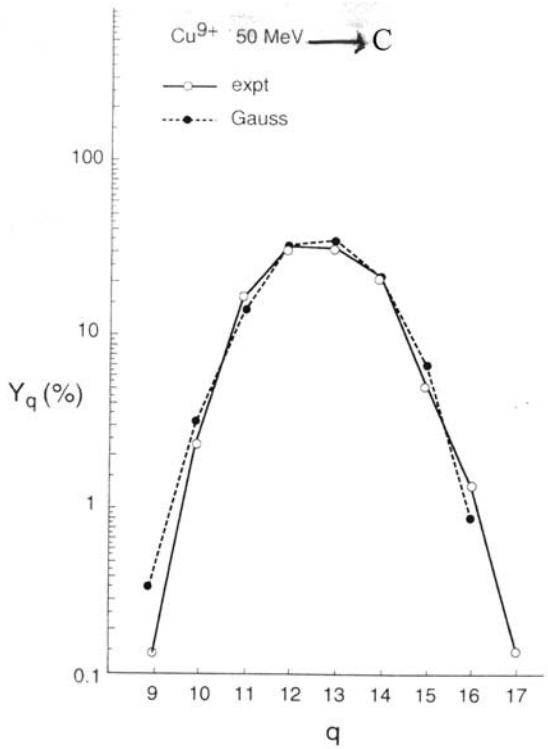

$$-\frac{dE}{dx} = \frac{4\pi N_0 e^4 \rho}{A_T m_e V_1^2} Z_{eff}^2 (\bar{Z}\ln\Lambda_F + (Z_T - \bar{Z})\ln\Lambda_B)$$

$$\Lambda_B = \frac{2m_e \upsilon_1^2}{I_{av}}$$

$$\Lambda_F = \frac{2m_e \upsilon_1^2}{\hbar\omega_p}$$

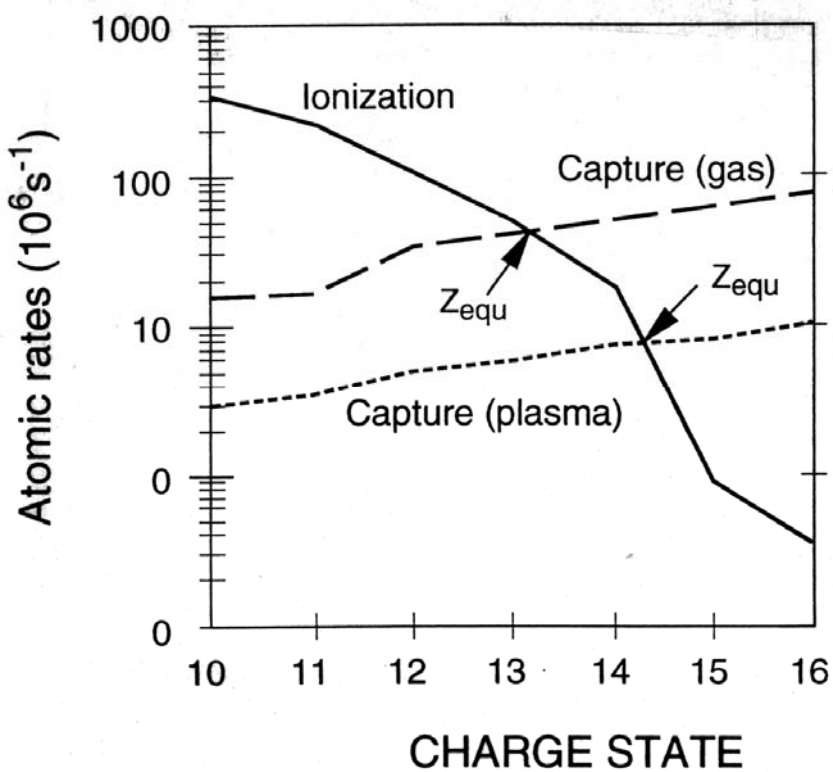

ION STOPPING IN DENSE PLASMA EXPERIMENTAL

$$\frac{\Delta E}{E} \cong \frac{n_e \ell}{E^2}$$

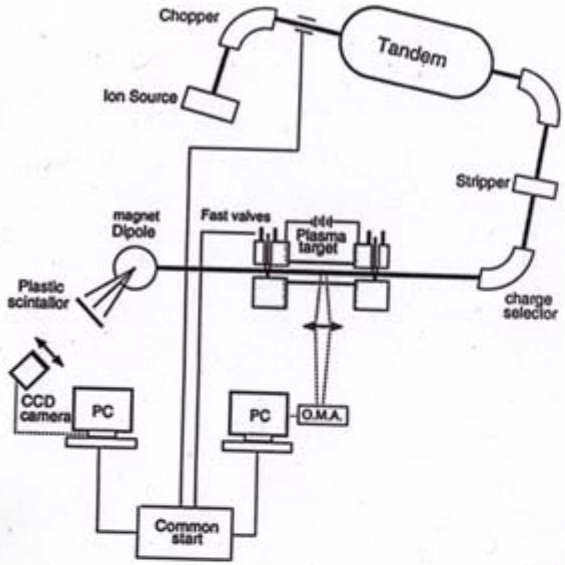

SPQR2

Orsay
Darmstadt
Moscow
Alma Ata
TIT

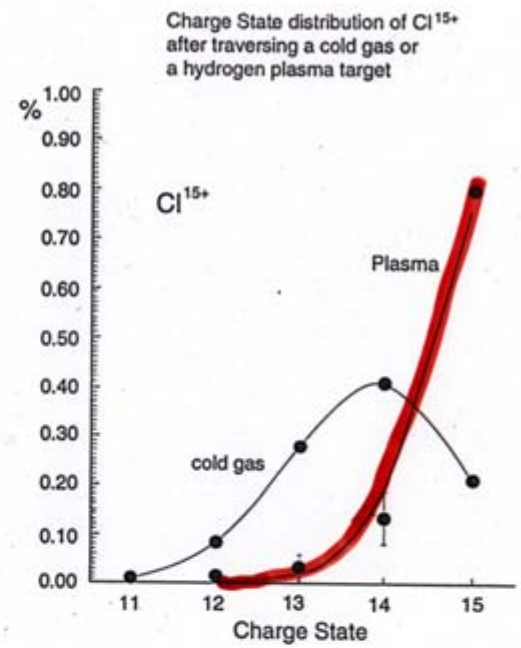

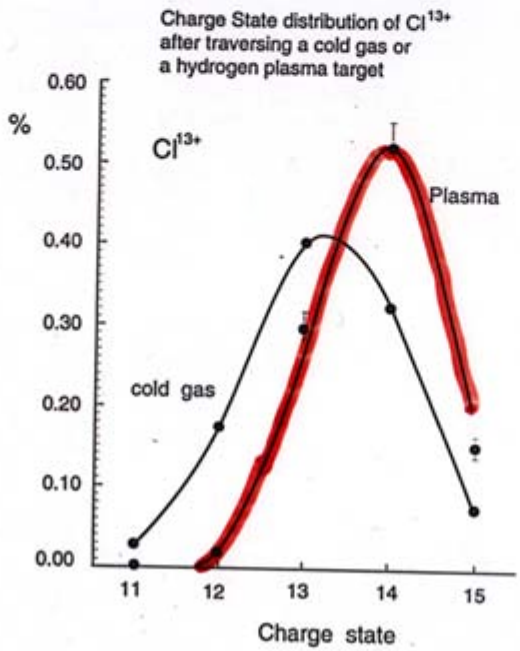

M. Chabot et al
Phys. Rev. E51, 3504 (1995)

$$\frac{\Delta E}{E} \cong \frac{n_e \ell}{E^2}$$

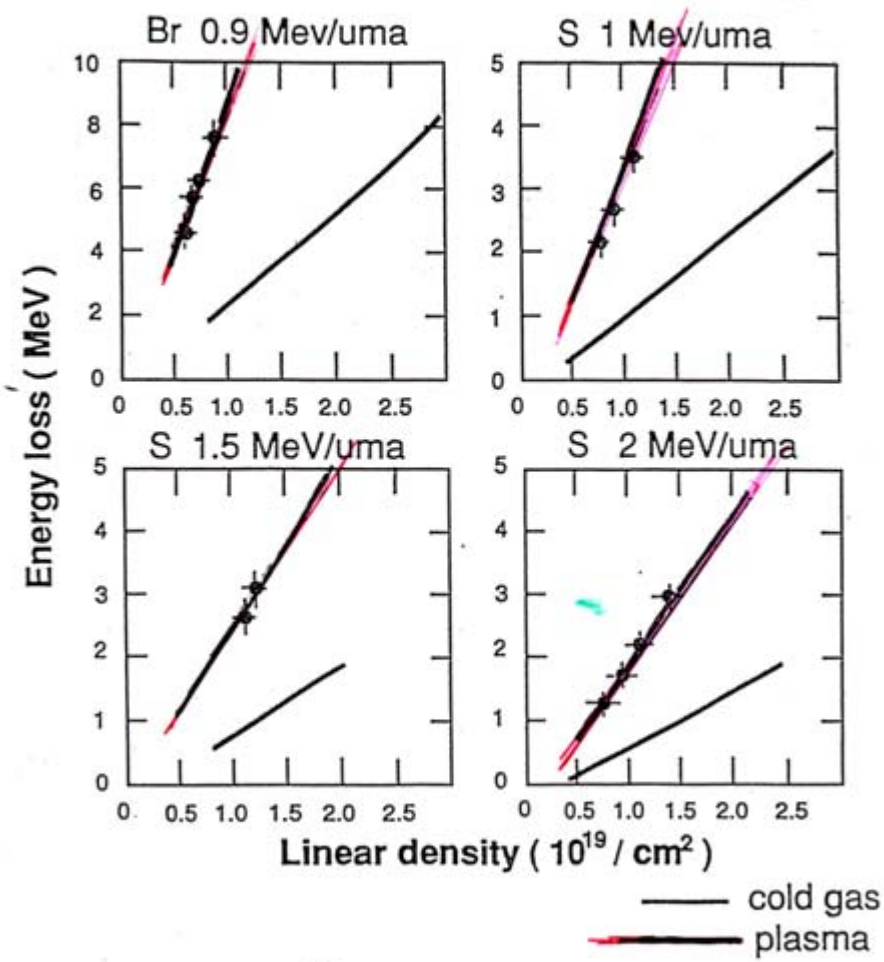

Orsay

NON LINEAR CORRECTIONS

Bloch term

Within the SSM framework outlined it is now straightforward to complete the stopping expression with Barkas ~ Z_p^3 and Bloch terms as well. In cold gas, those latter are no longer negligible when the Born parameter $Z_p V_0/(V_p^2+V_{th}^2)^{1/2}$ is comparable to 1. $V_0 = 1$ in atomic units. V_{th} is the thermal velocity of plasma electrons. Retaining also the very small target-ion contribution, one thus gets a more accurate stopping expression

$\sim Z_p^4$

SSM

Barkas

$$-\frac{dE}{dx}=\frac{4\pi N_0 e^4 \rho Z_p^2}{A_T m_e V_p^2}\, Z_T\left[\frac{\overline{Z}}{Z_T}L_0^F+\frac{Z_T-\overline{Z}}{Z_T}L_0^{\overline{B}}+Z_p\frac{V_0}{V_p}\right.,$$

Bloch

$$\left.+Z_p^2\frac{V_0^2}{V_p^2}\,f(V_p^2)+\frac{m_e}{A_T}Z_T L_p\right],$$

Ions

with

$$L_0^F=\mathrm{Ln}\frac{2m_e V_p^2}{\hbar\omega_p}-\frac{\langle V_{th}^2\rangle}{V_p^2}-\frac{\langle V_{th}^4\rangle}{2V_p^4}$$

and $\omega_p=\sqrt{4\pi e^2 n_e/m_e}$, the plasma frequency of the target free electrons.

Table 3.6

Relative importance of Bloch and Barkas terms for cold-gas and plasma target.
The target has a linear density of free electron $n_e = 1.5 \times 10^{19}$ cm^{-2}
[D. Gardès, G. Maynard *et al.*, *Phys. Rev.* **146**, 5101 (1992)]

		$\frac{Z_p V_0}{V_p}$		Bethe L_0		Barkas		Bloch	
Ion	E (MeV/amu)	Gas	Plasmas	Gas	Plasmas	Gas	Plasmas	Gas	Plasmas
C^{4+}	2	0.56	0.62	5.63	12.48	0.08	0	-0.3	-0.35
S^{7+}	1	1.75	2.07	4.94	11.79	0.35	0	-1.16	-1.32
	1.5	1.43	1.69	5.34	12.2	0.23	0	-0.98	-1.13
	2	1.24	1.47	5.63	12.48	0.18	0	-0.85	-1.00
Br^{6+}	0.93	2.79	3.45	4.86	11.72	0.64	0	-1.61	-1.82

Strategy: maximize uniformity and the efficient use of beam energy by placing center of foil at Bragg peak

In simplest example, target is a foil of solid or "foam" metal

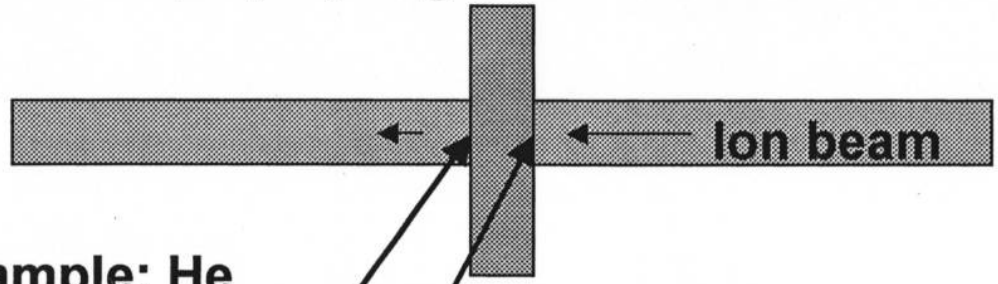

Example: He

Energy loss rate

$$-\frac{1}{Z^2}\frac{dE}{dX}$$

(MeV/mg cm²)

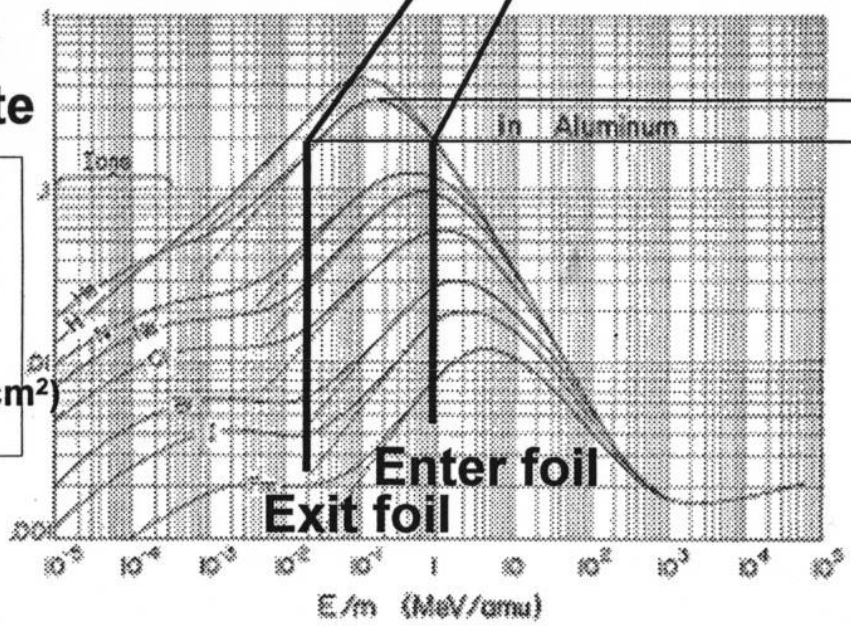

Energy/Ion mass (MeV/amu)

$\Delta dE/dX \propto \Delta T$

log-log plot => fractional energy loss can be high and uniformity also high if operate at Bragg peak (Larry Grisham, PPPL)

(dEdX figure from L.C Northcliffe and R.F.Schilling, Nuclear Data Tables, **A7**, 233 (1970))

Multiple scattering of slow ions in a Partially Degenerate Electron Fluid

A. SINGLE SCATTERING

Adapting the T = 0 formalism (cf. [14] and [6] for the ion projectile scattering probability expressed as

$$\frac{d^4P}{d^3q d\omega} = \frac{|F(q)|^2}{\pi^2 q^2} \; \mathrm{Im}\left[\frac{-1}{\varepsilon(q,\omega)}\right] \delta(\hbar\omega - \hbar\vec{q}.\vec{v}_p),$$

with a pointlike projectile form factor F(q) = Ze, Z being the ion charge, and using the splitting $d^3q = d^2q_\perp \, dq_{//}$ relative to initial beam velocity v_p we get

$$\frac{d^2P}{d^2q_\perp} = \int \frac{d^3P}{d^3q} dq_{//} \; .$$

$$= \frac{1}{\hbar\pi^2} \int \frac{dq_{//}}{q_\perp^2 + q_{//}^2} \; |F(q)|^2 \; \mathrm{Im}\left[\frac{-1}{\varepsilon(q,\omega)}\right]_{|\omega = q_{//} v_p} \; .$$

expressing the probability of ion projectile differential scattering yielding its angular deflections in single scattering events, through inclusion of the target electrons collective screening properties yields

$$\frac{dP}{dq_\perp} = v_p \times G_{\forall T}(q_\perp) \; .$$

where

$$G_{\forall T}(q_\perp) = \frac{4Z^2 e^4 m_e^2}{\hbar^4 \pi} \cdot q_\perp \cdot \int_{q_\perp}^{\infty} \frac{1}{(q^2 + q_s^2)^2} \cdot \frac{1}{1 + \exp(\frac{\hbar^2}{8 m_e T} q^2 - \eta)} dq \; ,$$

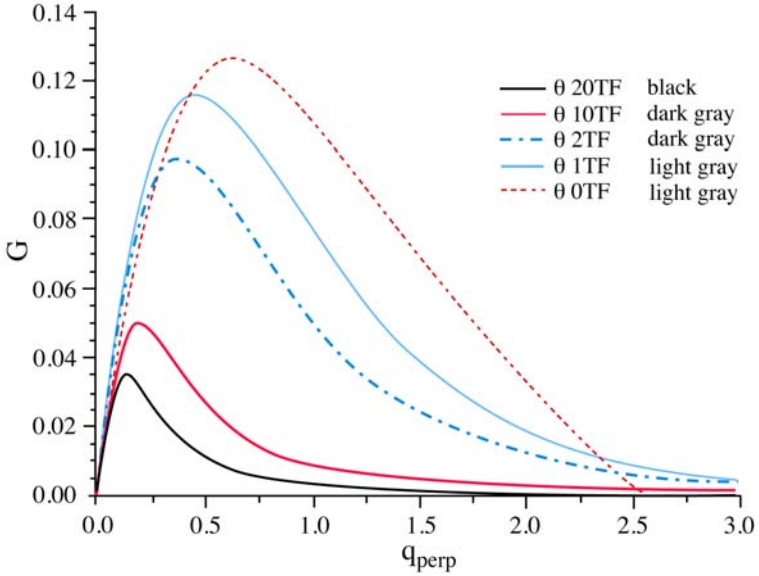

Probability distribution $G_{\forall T(q_\perp)}$ at any temperature T contrasted to its free electron gas (FEG) counterpart (T=0). $q_\perp$ in a_0^{-1} and r_s = 1.5).

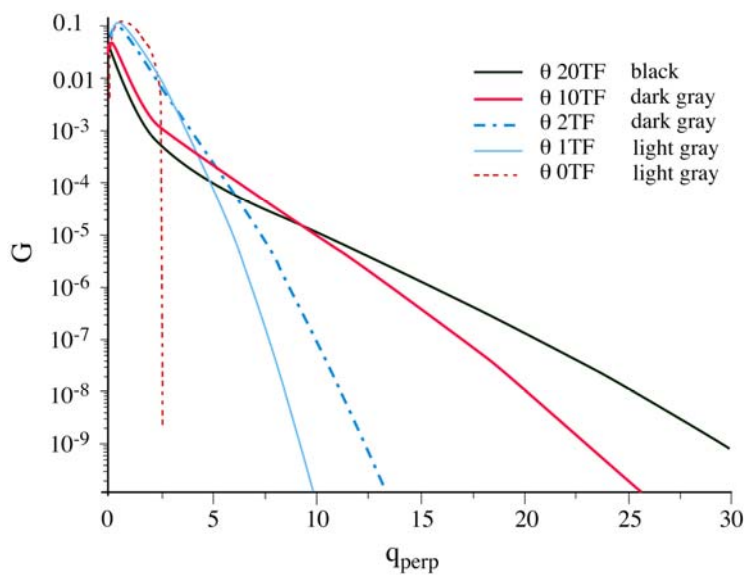

Same caption with enlarged q_{perp} range.

B- MULTIPLE SCATTERING

Général

From the density probability function we can access the differential cross-section for ion multiple scattering in a PDEF (Partially Degenerate Electron Fluid). At a given transverse momentum transfer $\hbar q_\perp$, this quantity writes as

$$d\sigma = \frac{1}{n_e v_p} dP = \frac{1}{n_e} \cdot G_{\forall T}(q_\perp) \tag{6}$$

with angular ion deflection ψ taken in the small-angle approximation $\hbar q_\perp = M_p v_p \psi$, with the ion projectile mass M_p.

We then turn to the convolution of the multiple scattering events, as the particle penetrates a distance X within the solid. It is usually represented by the multiple-scattering (MS) function $f(\alpha,X)$ which yields the statistical distribution of particles with a total angular deflection . So we can express the electronic multiple-scattering (EMS) function in the form $F(\alpha,X)d\Omega = f(\alpha,X)d\Omega/2\pi$, where $f(\alpha,X)$ is given in the small-angle approximation by

$$f(\alpha,X) = \int_0^\infty \kappa d\kappa J_0(\kappa\alpha) \exp^{-n_e X \sigma_0(\kappa)} \tag{7}$$

The function $\sigma_0(\kappa)$ defined scatterin is determined from the previously g function $G_{\forall T}(q_\perp)$, for the present case of a PDEF, which takes the form

$$\sigma_{0\forall T}(\kappa) = \int [1 - J_0(\kappa\psi)] d\sigma \ ,$$

$$= \frac{1}{n_e} \int_0^\infty \left[1 - J_0\left(\frac{\kappa q_\perp \hbar}{M_1 v_p}\right)\right] \cdot G_{\forall T}(q_\perp) dq_\perp \ , \tag{8}$$

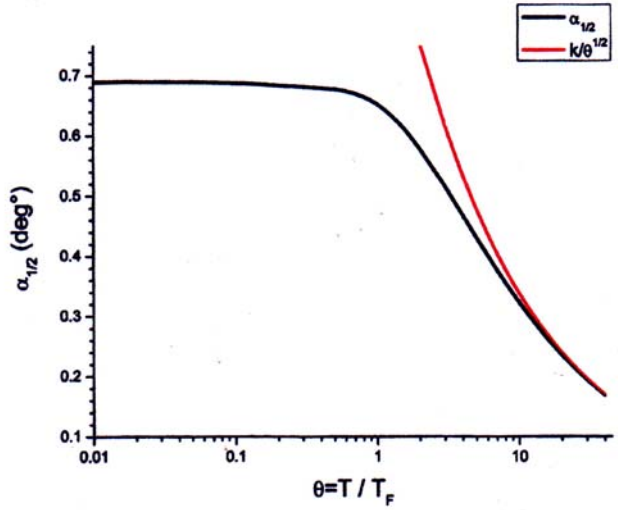

$\alpha_{1/2}$ (in degrees) in terms of T/T_F in an electron target with density $r_s = 1.5$ and thickness X = 800 a.u. (0.0424 μm). $k \approx 1$.

with $q_\perp$ qualifying a classical and non-degenerate upper bound. In this connection, it is worthwhile to notice that replacing the given infinite upper limit by the fully degenerate $2q_F$ one, does not change significantly $\sigma_0(\kappa)$ estimate.

Finally we reach the angular distribution function explained at Eq. (12) for a given penetration depth X in target.

HWHM angle $\alpha_{1/2}$

Analysis of quadrature of the previous reached essentially relies on $\alpha_{1/2}$, the half-angle at half-maximum, fulfilling $f(\alpha,X) = f(0,X)/2$. The usefulness of this concept is successively highlighted through its T-dependence, X-dependence, v_p-dependence as well as n_e (or r_s)-dependence.

The T-dependence is documented as a monotoneous decay for a PDEF target $\theta \geq 1$ with $n_e \approx 4.8 \times 10^{23}$ and a thickness X = 0.0424 μm (800 a.u.), while the strongly degenerate regime ($\theta < 1$) features a nearly horizontal plateau.

Proton beams may miss the target through multiple scattering

10 ps

$$\frac{\Delta E_p}{E_p} \leq 2(t_{Stag} - t_{LPS})\frac{V_p}{D}$$

20 ps

Ex : E_p = 15 MeV $\longrightarrow$ $\Delta E_p \leq$ 5.4 MeV for D = 3 mm

When the LPS is put outside the capsule, with a 30μm protecting gold foil, the transverse dispersion is rather large

E_p=15 MeV, D = 2.7 mm, 30μm gold foil,
99% of the protons are outside Rc (16μm)

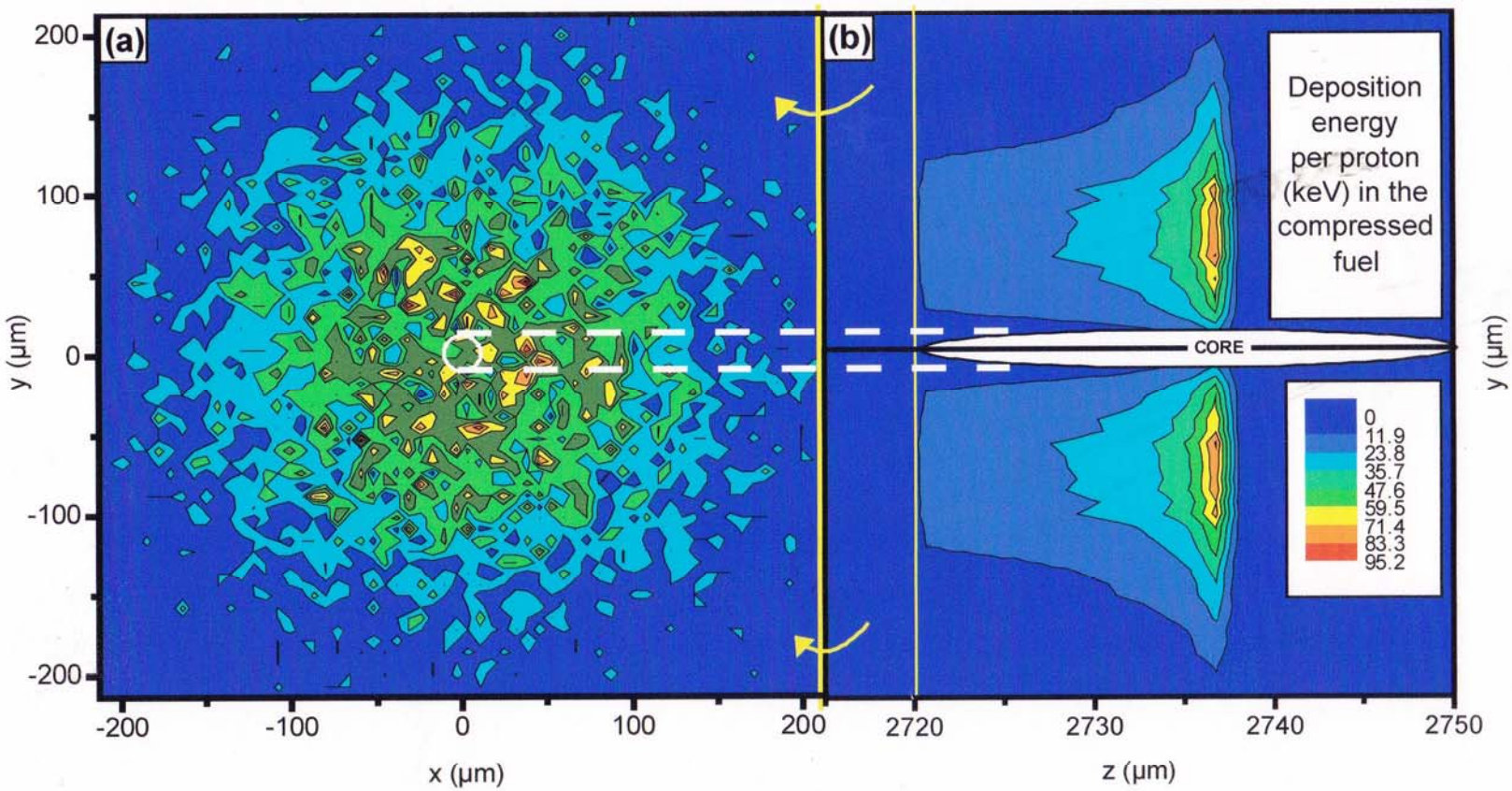

M. BARRIGA-CARRASCO, G. MAYNARD

Even for a protecting foil close to the target, the dispersion is large, when considering a broad energy distribution

D=0.5 mm, 30 µm gold foil, energy distribution of present LULI source

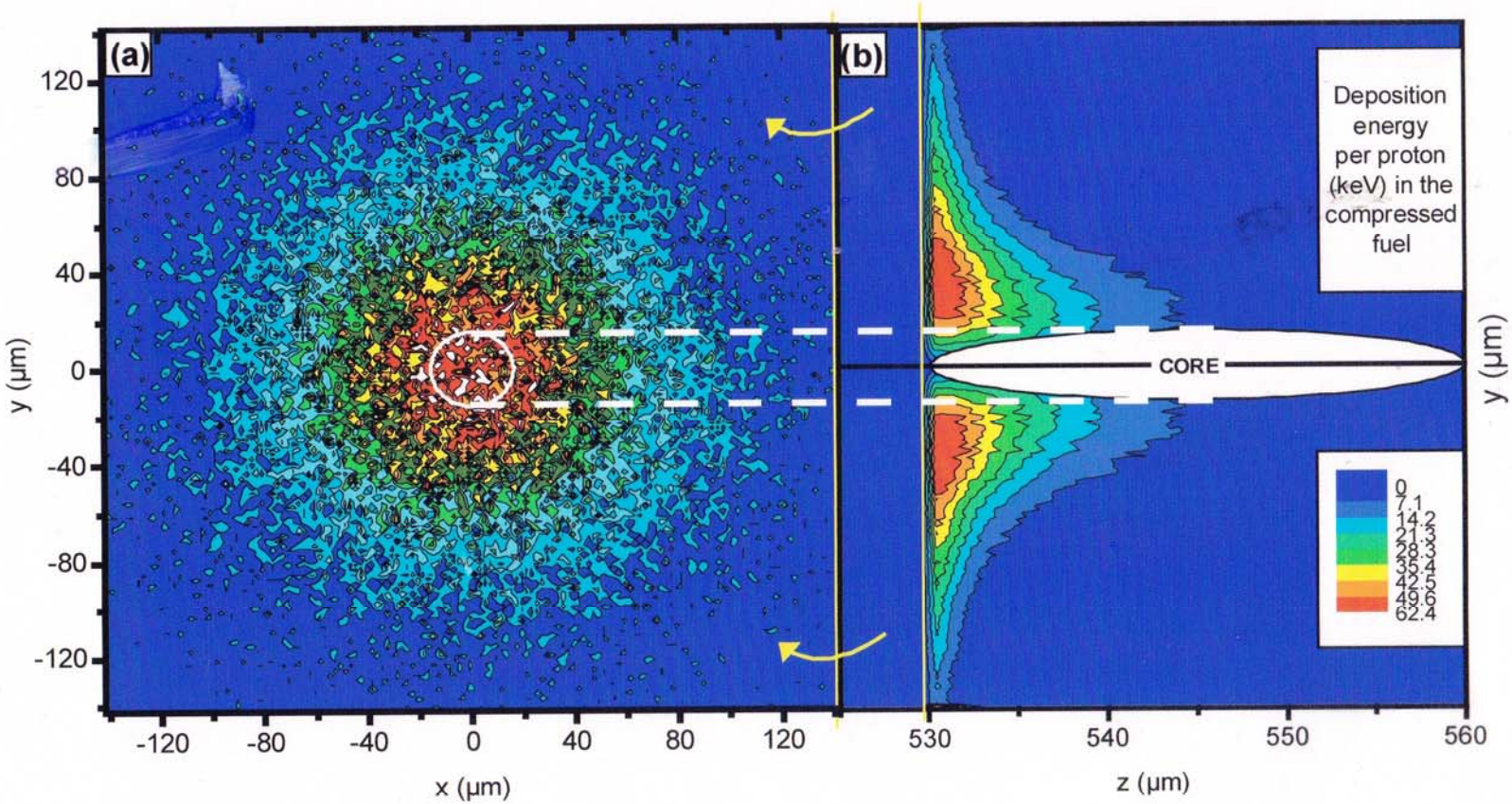

M. BARRIGA-CARRASCO, G. MAYNARD

Efficiency of energy deposition can be estimated through a simple formula for the width of the distribution in the transverse plane

$$\sigma(\mu m) = 0.07 \frac{\sqrt{\delta(\mu m)}(D + \delta)(\mu m)}{E_p(MeV) - 0.15\delta(\mu m)/E_p(MeV)}$$

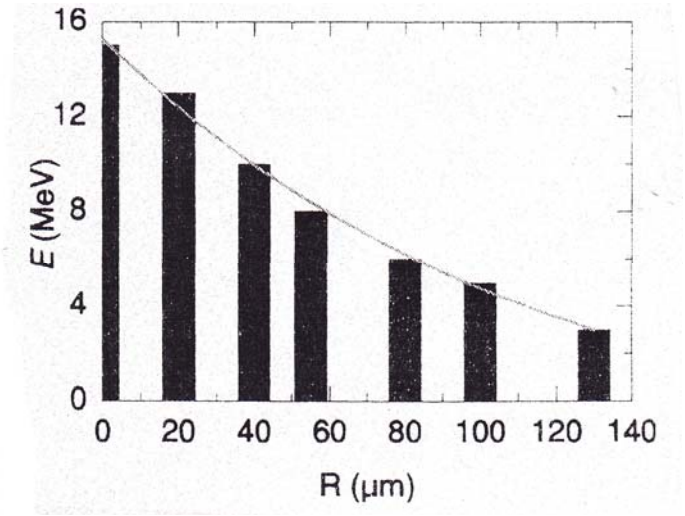

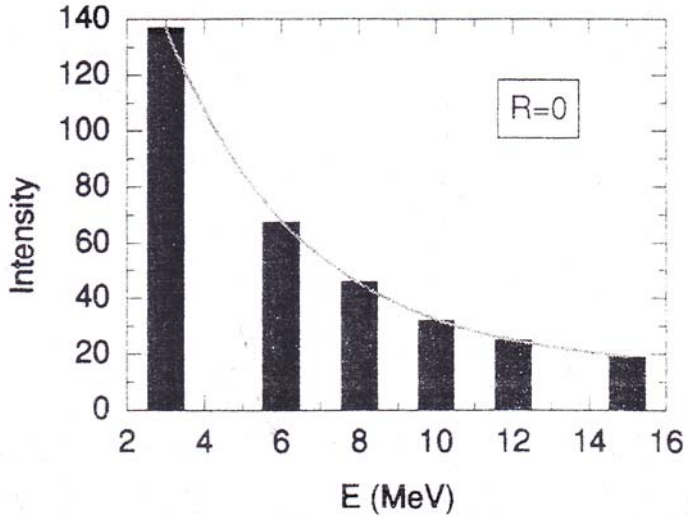

Typical example of the energy distributions of a proton beam with radius R generated by a LPS created by the 30J. 300 fs pulse of the 100 TW laser, at LULI, Palaiseau.

BINARY and MULTI-IONIC MIXTURES

The basic LIVSD behavior is, as well-known of the form

$$-\frac{dE}{dx} = Av_p$$

in the low ion projectile velocity limit advocated previously with energy/nucleon E/A ≤ 100 keV/amu.

Within the dielectric framework of present concern, we consider the electromagnetic response of a target plasma built on electrons and ion species (Z_i, M_i). The target ion part is taken here as a weakly coupled binary ionic mixture (BIM), which will prove sufficient in the subsequent considered plasma targets. In such an approach, it appears useful to work wtih the overall dielectric function

$$\varepsilon(\vec{k},\omega) = 1 + \frac{1}{k^2}\left(W\left(\frac{W}{k}\right) + W\left(\sqrt{M_1}\frac{W}{k}\right) + W\left(\sqrt{M_2}\frac{W}{k}\right)\right)$$

with the usual Fried-Conte dispersion function W(Imζ ≥ 0)

$$W(\varsigma) = \frac{1}{\sqrt{2\pi}} \lim_{\nu \to 0+} \int_{-\infty}^{\infty} dx \frac{x e^{-x^2/2}}{x - \varsigma - i\nu}$$

and X(ζ)=ReW(ζ), Y(z)=ImW(ζ).

Cf P. Fromy, B. Tashev and C Deutsch. PRSTAB **13**, 101302 (2010) and EPL **92**, 15002 (2010)

Generalizing the standard one-component stopping quadrature

$$-\left[\frac{dE}{dx}\right]=\frac{Z^2 N_D}{(2\pi)^2}\int_0^{k_{max}} dk\ k^3\int_{-1}^{+1} d\mu\frac{\mu Y(\mu v_p)}{\left[k^2+X(\mu v_p)\right]^2+Y^2(\mu v_p)}$$

with $Z = Z_{eff}/N_D$, where Z_{eff} denotes the projectile effective charge at velocity v_p, $N_D=n_e\lambda^3_{De}$ in terms of target electron density and corresponding Debye length. In the sequel, v_p will be scaled by , thermal electron velocity with T, thermalized target temperature.

$$k_{max}=\mathrm{Min}\left(\frac{m(v_p^2+v_{the}^2)}{Z_{eff}\ e^2},\ \frac{2m\sqrt{v_p^2+v_{the}^2}}{\hbar}\right)$$

$$=\mathrm{Min}\left(\frac{4\pi}{Z}(v_p^2+2),\ 8\pi\sqrt{2N_D}\frac{\alpha c}{v_{the}}\sqrt{v_p^2+2}\right)$$

Where v_p is now dimensionless on the second line on the right-hand-side. α=1/137 is the fine structure constant, and c, light velocity.

In adapting to BIM stopping, it proves convenient to introduce the relative ion concentration of species 1, i.e

$$\alpha=\frac{N_1}{N_1+N_2}$$

in terms of ion number N_i with i = 1,2, in target plasma, so that BIM densities

$$n_1=\frac{n_e\alpha}{\overline{Z}}\,,\quad n_2=\frac{n_e(1-\alpha)}{\overline{Z}}\,,\quad \overline{Z}=Z_1\alpha+Z_2(1-\alpha)$$

are straightforwardly expressed in terms of electron density n_e.

Then, we can estimate the stopping contributions of every target component : electron (0), ion 1 and ion 2 as follows

$$-\frac{dE_0}{dx}=C_0\int_0^{k_{max0}}dk\;k^3\int_{-1}^{+1}d\mu\frac{\mu Y[\mu v]}{D[k,\mu v]}$$

$$-\frac{dE_1}{dx}=C_1\int_0^{k_{max1}}dk\;k^3\int_{-1}^{+1}d\mu\frac{\mu Y\left[\sqrt{M_1}\,\mu v\right]}{D[k,\mu v]}$$

$$-\frac{dE_2}{dx}=C_2\int_0^{k_{max2}}dk\;k^3\int_{-1}^{+1}d\mu\frac{\mu Y\left[\sqrt{M_2}\,\mu v\right]}{D[k,\mu v]}$$

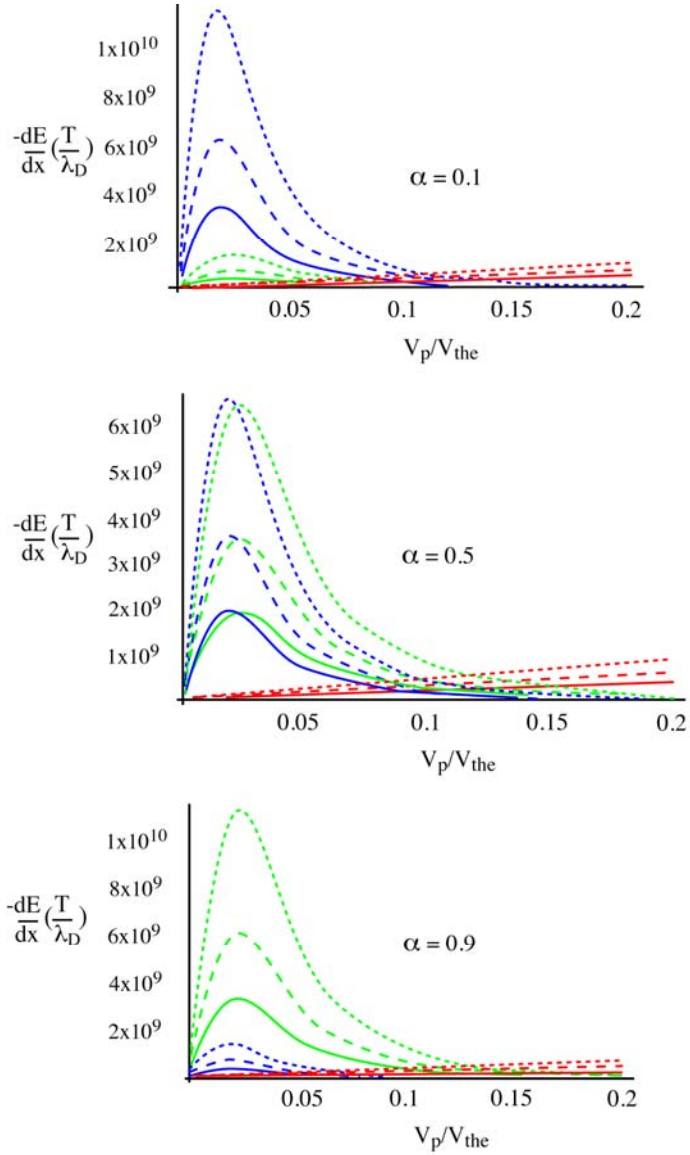

Figs. 3 - Proton stopping in a DT-mixture. $n_e = 10^{25}$ e-cm^{-3}

T(eV) = ····· 500, - - - - - 1000, —— 2000.

Red refers to e-stopping, green to D^+-stopping

and blue to T^+-stopping. $\alpha = D^+$-concentration.

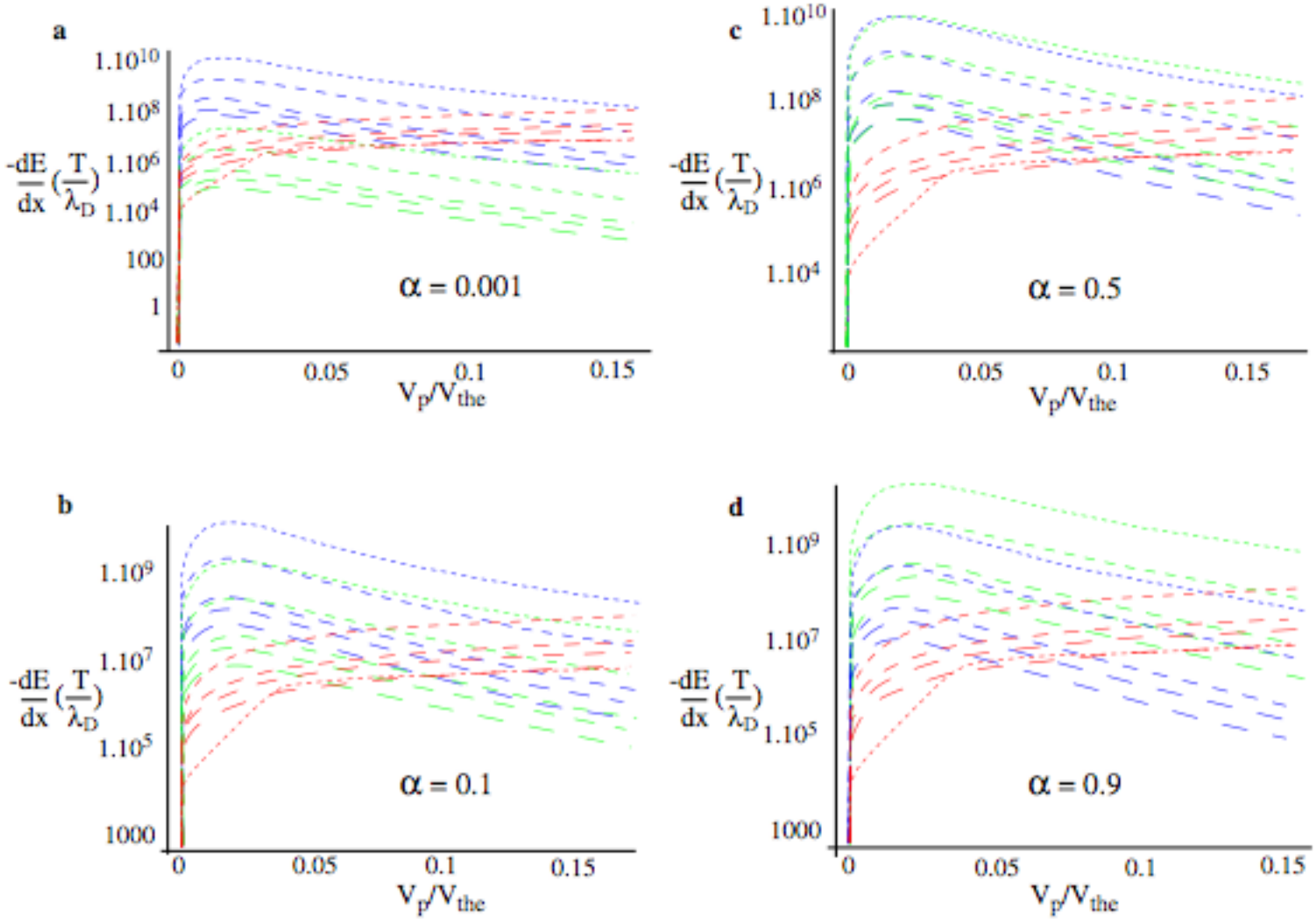

Figs. 4 - Alpha particle projectile in a Deuterium-Tritium BIM with $n_e = 10^{23}$ e-cm^{-3} and temperatures
= ····· 10 eV, - - - - - 100 eV, – – – – · 1 keV, — — — — 2 keV, — — — 5 KeV
with D^+ relative proportion **a)** $\alpha = 0.001$, **b)** $\alpha = 0.1$, **c)** $\alpha = 0.5$ and **d)** $\alpha = 0.9$.
Red refers to electron stopping, green to D^+-stopping while blue denotes T^+-stopping, $-dE/dx\ (T/\lambda_D)$ in terms of v_p/v_{the}.

Proton Stopping in polyimide (Kapton)

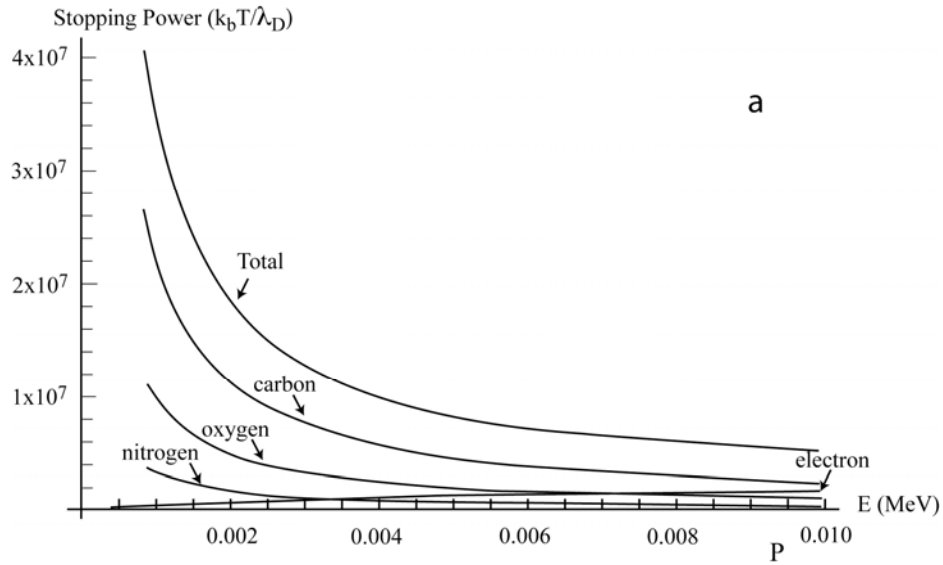

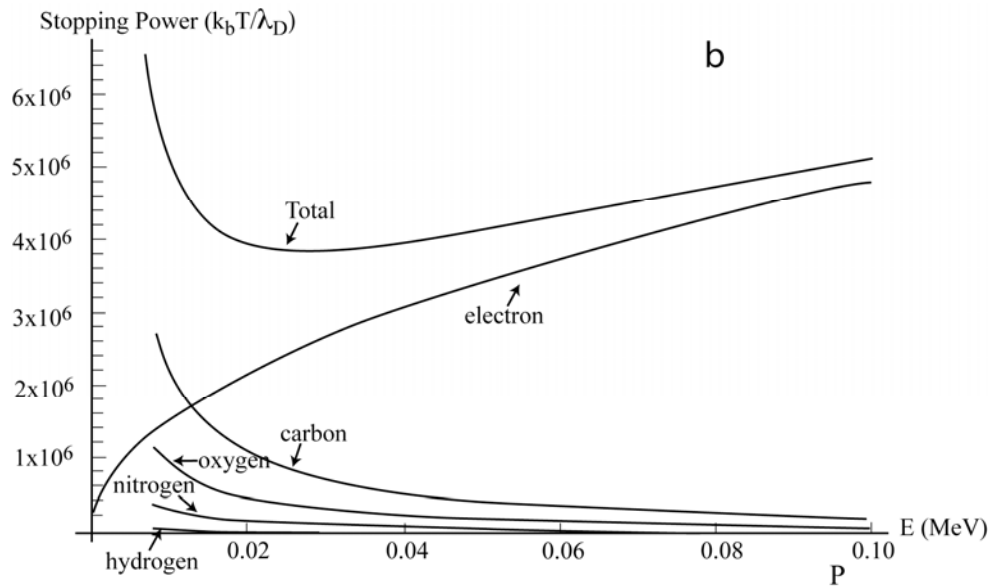

Proton stopping in Kapton at 0.1 g/cc and 1 keV. $Z_H = 0.99992$, $Z_C = 5.9845$, $Z_N = 6.69839$, and $Z_0 = 7.9766$

(a) Maximum E_P (MeV) = 0.01, (b) Maximum E_P(MeV) =0.1

Low Velocity Ion Slowing Down in a Demixing Binary Ionic Mixture

We consider ion projectile slowing down at low velocity Vp < Vthe, target thermal electron velocity, in a strongly coupled and demixing H-He ionic mixture. It is investigated in terms of quasi-static and critical charge-charge structure factors. Non-polarizable as well as polarizable partially degenerate electron backgrounds are given attention. The low velocity ion slowing down turns negative in the presence of long wavelength and low frequency hydromodes, signaling a critical demixtion. This process documents an energy transfer from target ion plasma to the incoming ion projectile.

Whitin a dielectric framework for target particles, the nonrelativistic ion stopping thus reads as

$$S = -\frac{dE}{dx} = -\frac{1}{V_p}\left(\frac{dE}{dt}\right)_0 = \frac{2}{\pi}\left(\frac{Z_p e}{V_p}\right)^2 \int_0^\infty \frac{dq}{q} \int_o^{qV_p} d\omega\omega \, \mathrm{Im}\left(-\frac{1}{\varepsilon(q,\omega)}\right) ,$$

which can be straightforwardly reexpressed in terms of the ion charge-ion charge structure factor when switching to very low

$$V_p \le \overline{V_{thi}} = C_1 V_{th1} + C_2 V_{th2} ,$$

with V_{thi}, thermal velocity and C_i, relative concentration of ion i.

$$S = \frac{2}{\pi}\left(\frac{Z_p e}{V_p}\right)^2 \int_0^\infty \frac{dq}{q} \int_o^{qV_p} d\omega \frac{4\pi^2 e^2 \omega}{\hbar q^2} \, S_{zz}(\vec{q},\omega)\left(e^{\beta\hbar\omega} - 1\right) ,$$

with the usual electron $\varepsilon(q,\omega)$ now extended to the ion components building up the BIM, and the charge-charge structure factor

$$S_{zz}(q) = \sum_{\alpha,\beta=1}^{2} (c_\alpha c_\beta)^{1/2} Z_\alpha Z_\beta S_{\alpha\beta}(q) ,$$

where $C_1+C_2 = 1$. C_i refers to concentration of species i within a BIM built on target ion charges Z_1 and Z_2.

Focussing attention on the slow and long wavelength hydromodes $\omega\to 0$, $q\to 0$ monitoring BIM demixing, one can safely restrict Eq. (1) to its static limit $\omega\to 0$

$$S = \frac{8\pi}{3}\left(Z_p e^2\right)^2 \beta V_p \int_0^\infty dq S_{zz}(q) \qquad (1)$$

Critical S_{zz} (q)

Mean field classical description of BIM demixing could be rather straightforwardly explained with the static charge-charge structure factor

$$S_{ZZ} = \frac{\Sigma|t|^{-\gamma}(qa_i)^2}{3\overline{\Gamma}\overline{Z}^2\left((q\xi)^2+1\right)} \qquad (2)$$

where $t = \frac{T-T_c}{T_c}$, T_c = critical temperature, γ = 1 and ξ = ion-ion correlation length featuring $\lim_{|t|\to 0} \xi \to \infty$.

$\overline{Z} = C_1Z_1 + C_2Z_2$ and $\overline{\Gamma} = C_1\Gamma_1 + C_2\Gamma_2$.

$\sum$ denotes a constant normalizing factor accessed through the sum rule (q in $\overline{a_i}^{-1}$)

(where $\overline{a_i} = C_1a_1 + C_2a_2$)

$$\int_0^\infty dq q^2\left[S_{zz}(q) - \overline{z^2}\right] = -\frac{3\pi}{2},$$

where $\overline{z^2} = 1 + C_1C_2(Z_1 - Z_2)^2/\overline{Z}^2$.

Expression (2) mostly emphasizes long distance hydromodes, of significance at critical demixtion.

Paying a first attention to nonpolarizable BIM with a fixed and rigid electron background, the correlation length reads as

$$\left(\frac{\bar{a}_i}{\xi}\right)^2 = 3\bar{\Gamma}\bar{Z}^{-2}\frac{D_I}{D_R} \quad ,$$

where D_I and D_R respectively denote the $q \to 0$ limit of

$$D_I(q) = \bar{Z}^2 - C_1C_2\left[Z_1^2\hat{C}_{22}^R(q) + Z_2^2\hat{C}_{11}^R(q) - 2Z_1Z_2\hat{C}_{22}^R(q)\right] \quad ,$$

and

$$D_R(q) = 1 - c_1\hat{C}_{11}^R(q) - c_2\hat{C}_{22}^R(q) - c_1c_2\det\left|\hat{C}_{\alpha\beta}^R(q)\right| \quad ,$$

in terms of

$$\hat{C}_{\alpha\beta}^R(q) = \hat{C}_{\alpha\beta}(q) + Z_\alpha Z_\beta\hat{v}(q) \quad , \qquad (3)$$

$\hat{C}_{\alpha\beta}^R(q)$ denotes the partial direct correlation function, viewed in the Ornstein-Zernikc (OZ) equations

$$\hat{h}_{\alpha\beta}(k) = \hat{C}_{\alpha\beta}(q) + \sum_{\nu=1}^{2} c_\nu\hat{h}_{\alpha\nu}(q)\hat{C}_{\nu\beta}(q) \quad ,$$

The right hand side of Eq. (3) also features the dimensionless and screened Coulomb potential

$$\hat{v}(q) = \frac{4\pi\beta e^2\bar{n}_i}{k^2\varepsilon(q)} \equiv \frac{3\bar{\Gamma}}{\bar{a}_i^2}\frac{1}{k^2\varepsilon(q)} \quad ,$$

with the dimensionless static electron fluid dielectric function $\varepsilon(q)$. Close to criticality, one expects a characteristic diverging behavior of the correlation length, so that

$$\xi = \xi_0^{\pm}|t|^{-\nu} \quad , \quad t \to 0$$

with $\nu = 0.5$, in a standard mean field OZ approximation.

Superelastic LVISD

The introduction of expression (?) into Eq. (3), thus yields for $q\bar{a}_i \le 1$,

$$S = \frac{8\pi}{3}\left(Z_p e^2\right)^2 \cdot \frac{\beta V_p}{\bar{a}_i} \cdot \frac{\Sigma|t|^{-1}}{\overline{\Gamma Z}^2}\left(\frac{\xi}{\bar{a}_i}\right)^2 \left[1 - \mathrm{Tan}^{-1}\left(\frac{\xi}{\bar{a}_i}\right)\right] ,$$

demonstrating that ξ-diverging behavior is compensated by that in Eq. (?).

Now we pay attention to correlation length estimates by solving simultaneously OZ equs with the Hypernetted Chain (HNC) equations

$$g_{\alpha\beta}(r) = \exp\left[h_{\alpha\beta}(r) - (C^R_{\alpha\beta}(r)\right] ,$$

valid for any Γ_i values

Lindhard screening involves (cf Fig. 1)

$$\varepsilon(k) = \frac{k^2 + k_{TF}^2 g_L(x)}{k^2} ,$$

where $k_{TF} = \left(6\pi n_e e^2 / E_F\right)^{1/2}$ denotes the Thomas-Fermi wave vector and the function $g_L(x)$ depends only on the dimensionless variable $x = k/2k_F$, with

$$g_L(x) = \frac{1}{2} + \frac{1-x^2}{4x}\ell n\left|\frac{1+x}{1-x}\right| ,$$

RIGID ELECTRON NEUTRALIZING BACKGROUND

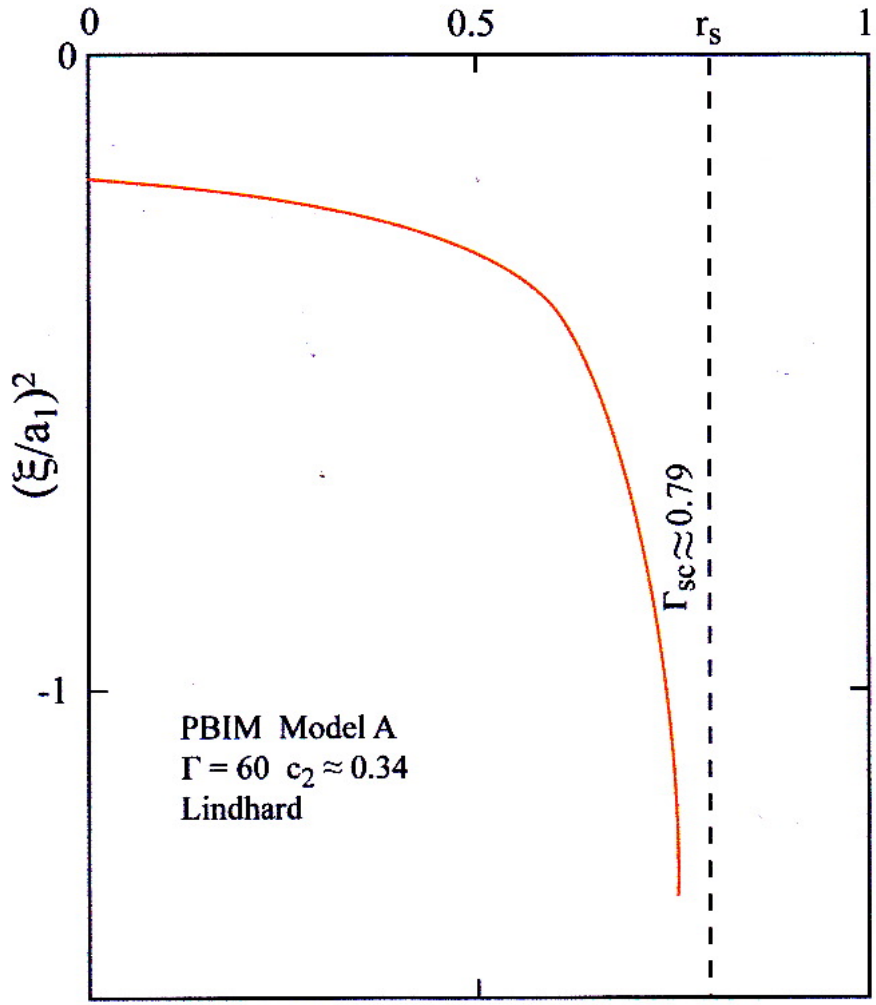

FIG. 1- Plot of the reduced squared correlation length $(\xi/a_1)^2$ in terms of r_s along a critical and vertical line (34% He, $\Gamma = 60$) with Lindhard screening. There ξ^2 remains negative.

UNPHYSICAL SITUATION

POLARIZED ELECTRON BACKGROUND

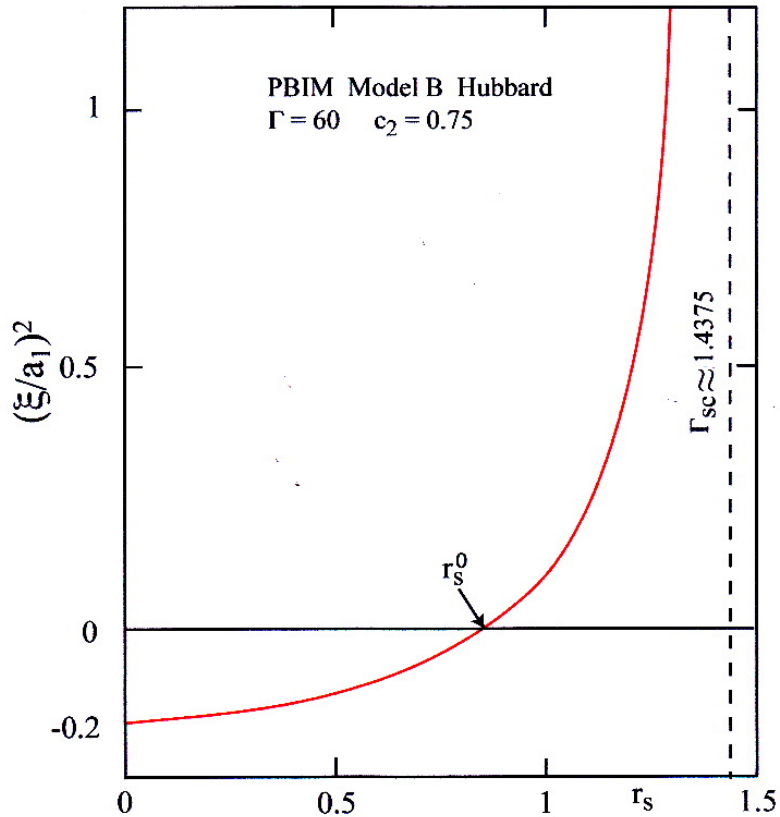

Fig. 2- PBIM model B with Hubbard screening. Plot of the reduced squared correlation length $(\xi/a_1)^2$ as a function of r_s along a critical and vertical line (75% He at $\Gamma = 60$) ξ^2 is now allowed to change sign for $r_s \geq r_s^0$.

On Fig.2 critical demixtion occurs at C_2=0.75 in lieu of C_2=0.34 on Fig. 1 for same $\Gamma = 60$. More importantly, ξ^2 is now allowed to increase positive on the largest r_s range side.

The resulting correlation length is now raising strongly when $|t| \rightarrow 0$, up to the standard mean field behavior $(\xi/a_1)^2 >> 1$.

The given LVISD is now negative featuring a superelastic interaction between the low velocity incoming ion projectile and the PBIMB target.

It can also be appreciated that before turning negative, LVISD vanishes for $(\xi/a_1)^2 \sim 1.65$.

FINAL REMARKS

The present development highlight for the first time the intriguing interplay of a first order demixing process in a strongly coupled and binary ionic mixture with a low velocity incoming ion beam. The latter may be envisioned for diagnostics purposes or target conditioning in the subfields of ICF and Warm Dense Matter, for instance.

Within a fundamental statistical physics perspective, it should be appreciated that the above results documents unambiguously the potentialities of probing collective very long wavelength phenomena occuring in a plasma target with low velocity ion beams via the evaluation of a transport coefficient, featured in the present context by a stopping power mechanism.